Liquid-Feed Flame Spray Pyrolysis as a Method of Producing Mixed-Metal Oxide Nanopowders of Potential Interest as Catalytic Materials. Nanopowders along the $NiO-Al_2O_3$ Tie Line Including $(NiO)_{0.22}(Al_2O_3)_{0.78}$, a New Inverse Spinel Composition

Jose A. Azurdia,[†] Julien Marchal,[†] Patrick Shea,[‡] Haiping Sun,[†] Xiaoqing Q. Pan,[†] and Richard M. Laine*,[†,§]

Departments of Materials Science and Engineering and Electrical Engineering and Computer Science and Macromolecular Science and Engineering, University of Michigan, Ann Arbor, Michigan 48109-2136

Received February 10, 2005. Revised Manuscript Received November 8, 2005

Liquid-feed flame spray pyrolysis (LF-FSP) is a general aerosol combustion route to unagglomerated and often single crystal mixed-metal oxide nanopowders with exact control of composition. LF-FSP of xNi$(O_2CCH_2CH_3)_2$/yAl$(OCH_2CH_2)_3$N EtOH solutions at selected x:y ratios provides mixed-metal oxide nanopowders with compositions covering much of the Al_2O_3-NiO phase space. All powders were characterized by XRD, BET, FTIR, SEM, TEM, and TGA-DTA. With the exception of pure NiO (specific surface area, SSA, ∼7 m^2/g), all product powders offer SSAs ≥ 45 m^2/g (average particle sizes ≤ 30 nm) without microporosity. At NiO/Al_2O_3 ratios near 1:1, the LF-FSP nanopowders are single phase, bright blue $NiAl_2O_4$ inverse spinel. The blue color of these materials is typical of Ni spinels. At higher NiO contents, NiO is the dominant phase with some δ-alumina and intermediate spinels. At low NiO contents, blue powders form but the δ-alumina phase predominates, suggesting incorporation of Ni^{2+} in the alumina lattice or formation of traces of $NiAl_2O_4$. Compositions near 20:80 mol NiO/Al_2O_3 generate an inverse spinel structure, per XRD with peaks shifted ≈4° 2θ to higher values from those of pure $NiAl_2O_4$. This contrasts with the published phase diagram, which suggests a mixture of $NiAl_2O_4$ spinel, and corundum should form at this composition. This material resists transformation to the expected phases on heating to 1400 °C, indicating a single stable phase which contrasts with the known phase diagram and, therefore, is a new material in $NiO-Al_2O_3$ phase space with potential value as a new catalyst.

Introduction

Numerous single and mixed-metal oxides, both pure and in supported forms, play important roles in commercial catalytic processes ranging from petroleum refining to environmental control, processing fine chemicals, andcomponents in fuel cells. Of the many catalyst systems studied extensively, nickel spinel and alumina supported nickel catalysts are among those that have widespread commercial value in catalytic applications ranging from methane/steam and methanol reforming[1−4] to hydrocarbon cracking, dehydrogenation, hydrodesulfurization, and hydrodenitrogenation.[5−8] Most recently, nickel spinel has received attention as an electrode material in high-temperature carbonate based fuel cells.[9,10]

Catalysts are prepared via a wide variety of methods including solid-state reactions, sol−gel processing, and incipient wetness and related support coating approaches.[11−15] Despite extensive studies designed to optimize synthetic methods in terms of surface areas, compositions, oxidation states, and so forth, there remains a need for general methods of preparing high surface area sinter-resistant catalysts that are easily manipulated for applications ranging from fluidized bed catalysis to simple supported liquid−solid and gas−solid catalysis. Such problems continue to exist for nickel spinel and alumina supported nickel catalysts.[16]

[†] Department of Materials Science and Engineering.
[‡] Department of Electrical Engineering and Computer Science.
[§] Macromolecular Science and Engineering.

(1) Lemonidou, A. A.; Goula, M. A.; Vasalos, I. A. *Catal. Today* **1998**, *46*, 175.
(2) Shaikhutdinov, S. K.; Avdeeva, L. B.; Goncharova, O. V.; Kochubey, D. I.; Novgorodov, B. N.; Plyasova, L. M. *Appl. Catal., A* **1995**, *126*, 125
(3) Matsumura, Y.; Nakamori, T. *Appl. Catal., A* **2004**, *258*, 107.
(4) Levent, M.; Gunn, D. J.; El-Bousiffi, M. A. *Int. J. Hydrogen Energy* **2003**, *28*, 945.
(5) Chokkaram, S.; Srinivasan, R.; Milburn, D. R.; Davis, B. H. *J. Mol. Catal. A: Chem.* **1997**, *121*, 157.
(6) Salagre, P.; Fierro, J. L. G.; Medina, F.; Sueiras, J. E. *J. Mol. Catal. A: Chem.* **1996**, *106*, 125.
(7) Rodríguez, J. C.; Marchi, A. J.; Borgna, A. Monzon, A. *J. Catal.* **1997**, *171*, 268.
(8) Kaewpuang-Ngam, S.; Inazu, K.; Kobayashi, T.; Aika, K.-I. *Water Res.* **2004**, *38*, 778.
(9) Wijayasinghe, A.; Kagergren, C.; Bergman, B. *Fuel Cells* **2002**, *2*, 181.
(10) Kou, L.; Selman, J. R. *J. Appl. Electrochem.* **2000**, *30*, 1433.
(11) Han, Y. S.; Li, J. B.; Ning, X. S.; Yang, X. Z.; Chi, B. *Mater. Sci. Eng., A* **2004**, *369*, 241.
(12) Areán, C. O.; Mentruit, M. P.; López, A. J.; Parra, J. B. *Colloids Surf., A* **2001**, *180*, 253.
(13) Schmidt, W.; Weidenthaler, C. *Chem. Mater.* **2001**, *13*, 607.
(14) Jeevanandam, P.; Koltypin, Y.; Gedanken A. *Mater. Sci. Eng., B* **2002**, *90*, 125.
(15) Amini, M. M.; Torkian, L. *Mater. Lett.* **2002**, *57*, 639.
(16) Mariño, F.; Baronetti, G.; Jobbagy, M.; Laborde, M. *Appl. Catal., A* **2003**, *238*, 41.

10.1021/cm0503026 CCC: $33.50
Published on Web 01/06/2006

Phase pure nickel spinels with controlled stoichiometries are very difficult to synthesize by traditional methods because of the very high temperatures required to obtain sufficient solid-state diffusion to drive the reaction to completion.[17−19] Liquid-feed flame spray pyrolysis (LF-FSP) provides a simple route to nanopowders of all compositions along the $NiO-Al_2O_3$ tie line with excellent control of stoichiometry, phase, and high surface areas without microporosity. This work extends the utility of LF-FSP as a means of producing a wide variety of mixed-metal oxide nanopowders with limited aggregation, complete control of stoichiometry, selected control of phase purity, and good-to-excellent handling characteristics.[20−25]

The LF-FSP process aerosolizes alcohol solutions of single or multiple alkoxides and/or carboxylates with oxygen and combusts the aerosol within a quartz chamber. Combustion produces flame temperatures of 1500−2000 °C depending on the processing conditions and ceramic oxide soot with stoichiometries identical to those in the original solution.[20−25] These soots, produced in 30−300 g/h rates, consist of single and mixed-metal oxide nanopowders (10−100 nm average particle sizes, APS) with specific surface areas (SSAs) of 30−100 m^2/g, good dispersibility and no microporosity with excellent control of chemical and phase composition. To this end, we recently reported detailed studies on LF-FSP syntheses of nano-δ-alumina, rare-earth doped δ-alumina laser materials, ion-conducting sodium doped β''-Al_2O_3, and materials along the $TiO_2-Al_2O_3$ tie line designed to identify potentially novel photocatalysts.[20−25] LF-FSP of $Y_3Al_5O_{12}$ composition nanopowders does not give the traditional YAG phase but a denser, new Perovskite phase.[21a]

These studies provide the background for efforts initiated here to develop new types of single-phase catalyst systems using LF-FSP. Complimentary work on the use of LF-FSP to synthesize phase-segregated catalysts has been described by Baiker et al.[26−29] Here we explore $NiO-Al_2O_3$ phase space with the goal of demonstrating that LF-FSP offers the potential to generate novel, single-phase forms of catalytic materials, which contrasts with earlier efforts in this field which suggest that it is difficult to form phase pure nickel spinels.[30−40] In this light, we also report on the hitherto unknown and thermally stable inverse nickel spinel, $(NiO)_{0.22}$-$(Al_2O_3)_{0.78}$.

In future papers, we will discuss LF-FSP studies along the $CeO_2-Al_2O_3$, $ZrO_2-Al_2O_3$ tie lines followed by studies on the ternary, $CeO_2/ZrO_2/Al_2O_3$, and quaternary, $CeO_2/ZrO_2/NiO/Al_2O_3$, systems where it is possible to generate three-way auto-exhaust washcoat materials and steam reforming catalysts in one step using LF-FSP.

Experimental Section

Materials. Nickel nitrate hexahydrate [$Ni(NO_3)_2 \cdot 6H_2O$, 99.9%], anhydrous ethanol and butanol, and triethanolamine [$N(CH_2CH_2OH)_3$, 98%] were purchased from Aldrich and used as received. Aluminum tris(*sec*-butoxide), [$Al(OsBu)_3$, 97%] was purchased from Chattem Chemical Co. Propionic acid [$C_2H_5CO_2H$, 99+%] was purchased from Alfa Aesar and also used as received.

Precursor Formulations. *Alumatrane.* Alumatrane was produced via a chemical route for the sake of high purity. A 4.2 L solution was synthesized from $Al(OsBu)_3$ and triethanolamine as described elsewhere[22] and then diluted in ethanol such that the solution thermogravimetric analysis (TGA) ceramic yield was 7 wt %.

$Ni(O_2CCH_2CH_3)_2$. $Ni(NO_3)_2 \cdot 6H_2O$ powder (75.0 g, 0.2579 mol) was placed in a 500 mL flask equipped with a still head, addition funnel, and a N_2 sparge. Propionic acid (250 mL, 3.40 mol) was added rapidly, and the resulting solution was heated to ∼150 °C for 4 h to distill off ∼140 mL of liquid (water/propionic acid) and coincidentally remove NO_x gas. The remaining liquid product was placed in a clean 500 mL Nalgene bottle. The ceramic loading of the solution was determined by TGA to be 9.7 wt %. This procedure was repeated twice to produce ∼450 mL of $Ni(O_2CCH_2CH_3)_2$, sufficient to produce all of the precursor samples. The solid nickel propionate was isolated by first washing the liquid precursor with ∼450 mL (1.75 mol) of tetrahydrofuran. The solution was slowly heated to distill off excess solvent and reactant. After the solution was reduced to ∼200 mL of a viscous green gel by a rotoevaporator, it was dried to a solid under a dynamic vacuum at 70 °C. The TGA of this product is discussed in Results and Discussion.

Eight different precursor formulations (Table 1) were prepared to study the $NiO-Al_2O_3$ phase space. Thus, precise amounts of alumatrane solution and nickel propionate solutions were mixed and diluted in ethanol to produce 4 wt % ceramic yield solutions. The samples produced were pure Al_2O_3; 3, 5, 22, 43, 63, and 78 mol % NiO; and pure NiO.

(17) Han, Y. S.; Li, J. B.; Ning, X. S.; Chi, B. *J. Am. Ceram. Soc.* **2004**, *87*, 1347.
(18) Subramanian, R.; Higuchi, M.; Dieckman, R. *J. Cryst. Growth* **1994**, *143*, 311.
(19) Cooley, R. F.; Reed, J. S. *J. Am. Ceram. Soc.* **1972**, *58*, 395.
(20) Sutorik, A. C.; Neo, S. S.; Treadwell, D. R.; Laine, R. M. *J. Am. Ceram. Soc.* **1998**, *81*, 1477.
(21) (a) Marchal, J.; John, T.; Baranwal, R.; Hinklin, T.; Laine, R. M. *Chem. Mater.* **2004**, *16*, 822. (b) Laine, R. M.; Youngdahl, K. A.; Kennish, R. A.; Hoppe, M. L.; Zhang, Z.-F. *J. Mater. Res.* **1991**, *6*, 895.
(22) Baranwal, R.; Villar, M. P.; Garcia, R.; Laine, R. M. *J. Am. Ceram. Soc.* **2001**, *84*, 951.
(23) Kim, S.; Gislason, J. J.; Morton, R. W.; Pan, X. Q.; Sun, H. P.; Laine, R. M. *Chem. Mater.* **2004**, *16*, 2336.
(24) (a) Hinklin, T.; Toury, B.; Gervais, C.; Babonneau, F.; Gislason, J. J.; Morton, R. W.; Laine, R. M. *Chem. Mater.* **2004**, *16*, 21. (b) Bickmore, C. R.; Waldner, K. F.; Baranwal, R.; Hinklin, T.; Treadwell, D. R.; Laine, R. M. *J. Eur. Ceram. Soc.* **1998**, *18*, 287. (c) Waldner, K.; Laine, R. M.; Bickmore, C. R.; Dumrhongvaraporn, S.; Tayaniphan, S. *Chem. Mater.* **1996**, *8*, 2850.
(25) Laine, R. M.; Marchal, J.; Sun, H. J.; Pan, X. Q. *Adv. Mater.* **2005**, *17*, 830.
(26) Stark, W. J.; Pratsinis, S. E. *Powder Technol.* **2002**, *126*, 103.
(27) Strobel, R.; Krumeich, F.; Stark, W. J.; Pratsinis, S. E.; Baiker, A. *J. Catal.* **2004**, *222*, 307.
(28) Fischer, A.; Mallat, T.; Baiker, A. *J. Mol. Catal. A: Chem.* **1999**, *149*, 197.
(29) Maris, M.; Mallat, T.; Orglmeister, E.; Baiker, A. *J. Mol. Catal. A: Chem.* **2004**, *219*, 371.
(30) Ata-Allah, S. S.; Fayek, M. K.; Refai, H. S.; Mostafa, M. F. *J. Solid State Chem.* **2000**, *149*, 434.
(31) Li, L.; Li, G.; Smith, R. L., Jr.; Inomata, H. *Chem. Mater.* **2000**, *12*, 3705.
(32) Wang, Z.; Saxena, S. K.; Lazor, P.; O'Neill, H. S. C. *J. Phys. Chem. Solids* **2003**, *64*, 425.
(33) Gabal, M. A. *J. Phys. Chem. Solids* **2003**, *64*, 1375.
(34) O'Neill, H. S. C.; Navrotsky, A. *Am. Mineral.* **1983**, *68*, 181.
(35) O'Neill, H. S. C.; Navrotsky, A. *Am. Mineral.* **1984**, *69*, 733.
(36) Cormack, A. N.; Lewis, G. V.; Parker, S. C.; Catlow, C. R. A. *J. Phys.* Chem. Solids **1988**, *49*, 53.
(37) Ivanov, V. V.; Talanov, V. M.; Shabel'skaya, N. P. *Inorg. Mater.* **2001**, *37*, 839.
(38) MacKenzie, K. J. D.; Cardile, C. M. *Thermochim. Acta* **1990**, *165*, 207.
(39) Lejus, A. M. *Rev. Int. Hautes Temp. Refract.* **1964**, *1*, 53.
(40) Colin, F. *Rev. Int. Hautes Temp. Refract.* **1968**, *5*, 267.

Table 1. NiO−Al_2O_3 Precursor Formulations[a]

sample	mol % NiO	moles Al_2O_3	moles NiO
1	0.0	0.098	0.000
2	3.2	0.954	0.029
3	5.3	0.933	0.051
4	22.2	0.806	0.228
5	43.5	0.622	0.475
6	62.8	0.446	0.717
7	77.9	0.270	0.955
8	100.00	0.000	0.133

[a] NiO precursor = $Ni(O_2CCH_2CH_3)_2$; Al_2O_3 = alumatrane.

LF-FSP. The LF-FSP apparatus has been described elsewhere in detail.[24] Typically precursor solutions are prepared with a 2−5 wt % ceramic yield, in EtOH or EtOH/MeOH or EtOH/^{n}BuOH mixtures.

The solutions are atomized at ∼60 mL/min using an oxygen atomizer to generate an oxygen rich aerosol that is ignited via methane−oxygen pilot torches in the device's combustion chamber.[20] Combustion occurs at temperatures > 1500 °C producing nanopowders and gaseous byproducts, which are carried downstream by a radial pressure blower at velocities in excess of 20 m^3/min. The powders are collected in electrostatic precipitators (ESP) maintained at a 10 kV direct current potential. After completion of a run, the powders are recovered from the ESP tubes and stored in plastic bags. The production rates are typically 30−300 g/h.

Analytical Methods. *Chemical Analyses*. Chemical analyses for LF-FSP samples were obtained independently by inductively coupled plasma (ICP) spectroscopy from Galbraith Laboratories (Knoxville, TN) and X-ray fluorescence (XRF) spectroscopy from Ford Motor Co. (Dearborn, MI). XRF samples were prepared by mixing 0.50 g of sample into 10.0 g of $Li_2B_4O_7$ glass flux. The sample and glass flux were mechanically stirred for 5 min in a methacrylate vial with three methacrylate balls using a SPEX 6000 ball mill. The mixtures were fused into glass beads by placing them in an oven held at 1000 °C for 10 min. The samples were analyzed using a Panalytical PW2400 XRF spectrometer (formerly Philips), equipped with a WDS detection system (wavelength dispersive), by Ford Motor Co. personnel.

TGA-Differential Thermal Analysis (DTA). Simultaneous TGA-DTA was performed on a SDT 2960 simultaneous TGA-DTA instrument (TA Instruments, Inc., New Castle, DE). Measurements were performed under a continuous flow of synthetic air (60 mL/min). The instrument was calibrated with gold supplied by Perkin-Elmer. Samples (40 mg) were hand pressed in a 3 mm dual action die, then placed in alumina sample cups with an empty alumina cup as the reference. Samples were heated at 10 °C/min to 1300 °C and then allowed to cool to ambient temperature at 20 °C/min.

Scanning Electron Microscopy (SEM). SEM micrographs were taken using a Philips XL30 scanning electron microscope (Philips, Germany). Powder samples were prepared by dispersing the powders in 5 mL of distilled water using an ultrasonic horn (Vibracell, Sonics and Materials, Inc., Newton, CT). A drop of the dispersion was then placed on aluminum stubs and placed on a covered hot plate to dry. The samples were sputter coated with a Technics Hummer VI sputtering system (Anatech, Ltd., Alexandria, VA) to improve contrast and conductivity with Ar for 2 min using an operating voltage of 10−30 kV while holding the chamber pressure below 10 mBar.

X-ray Diffraction (XRD) Analysis. The phases present and crystallite sizes of as-prepared samples were characterized by XRD, performed on a Rigaku Miniflex diffractometer (Rigaku Denki Co., Ltd., Tokyo, Japan). The samples were placed (∼100 mg) in amorphous silica sample holders. XRD continuous scans in a $\theta-2\theta$ configuration were made from 20 to 80° 2θ, using a scan rate of 2°/min in 0.05° increments and Cu Kα radiation ($\lambda = 1.54$ Å) with working voltage and current of 30 kV and 15 mA, respectively. Scan data was processed using Jade software version 3.1 (Materials Data, Inc., Livermore, CA). Peak positions and relative intensities were characterized by comparison with ICDD files 44-1159, 10-0339, 46-1215, and 46-1131 to identify the crystallographic phases and to determine the relative phase compositions. Peak broadening and pattern simulation was also used to confirm the APS obtained by surface area analysis. Instrumental broadening was not taken into account when making these calculations, but the machine manufacturer publishes a 0.3 2θ° broadening.

XRD analyses were also performed on a Philips X'Pert Pro[42] diffractometer. Powder samples were placed in a low background Si holder.[43] The diffractometer was operated at 40 kV and 40 mA, and the X-ray source was Cu radiation. The detector used was X'Celerator with receiving Soller collimators. Scans were acquired from 4 to 145° 2θ with an increment of 0.05° 2θ at 7.25° 2θ/min. Patterns were processed using Material Data, Inc.,[44] Jade version 6.1 and Riqas version 4.0.0.8 software packages. Peak positions and relative intensities were characterized by comparison with ICDD files as above. The starting conditions for the major five phases are listed in Table 2.

Surface Area Analysis. SSAs of the different samples were obtained using a Micromeritics ASAP 2010 sorption analyzer (Norcross, GA). Samples (∼200 mg) were degassed at 400 °C until the degas rate was less than 0.005 Torr/min. Analysis was conducted at −196 °C (77 K) with N_2 as the adsorbate gas. The SSAs were calculated using the BET multipoint method with at least 10 data points with relative pressures of 0.001−0.20. The particle average size was derived from the following:

$$r = \frac{3}{\rho \times \mathrm{SSA}}$$

where ρ is the theoretical density of the powders and r is the particle radius.

Vegard's Law Calculations. Vegard's law calculations were used to determine the cell parameters for sample 4. The end member values for the cell parameter calculation were pure $NiAl_2O_4$ spinel (0.8048 nm) and the arithmetic mean for the cell parameter of δ-Al_2O_3 and δ*-Al_2O_3 (0.7899 nm). The excess alumina (vs NiO) in the sample was calculated to be 31.7%. These are the values used in the linear interpolation formula.

Transmission Electron Microscopy (TEM). High-resolution TEM (HRTEM) images were acquired using a JEOL 4000EX (Osaka, Japan) electron microscope operated at 400 kV. Powder samples were prepared by dispersing ∼5 mg in 5 mL of 2-propanol using an ultrasonic water bath at room temperature for 5 min. A drop of the dispersion was then placed on holey carbon film on Cu grids, 300 mesh (SPI Industries, Indianapolis, IN) and placed on a covered hot plate to dry. Once dry, the samples were mounted on a Gatan double-tilt goniometer, to be imaged.

Diffuse Reflectance Infrared Fourier Transform Spectroscopy (DRIFTS). DRIFTS spectra were recorded on a Mattson Galaxy Series FTIR 3000 infrared spectrometer (Mattson Instruments, Inc., Madison, WI). Samples were prepared by grinding 400 mg of optical grade KBr (International Crystal Laboratories, Garfield, NJ) using an alumina mortar and pestle, and 4 mg (1.0 wt %) of sample

(41) Bassoul, P.; Gilles, J. C. *J. Solid State Chem.* **1985**, *58*, 383.
(42) Philips Analytical, P.O. Box 13, 7600 AA, Almelo, The Netherlands.
(43) The Gem Dugout, 1652 Princeton Drive, State College, PA 16803, U.S.A.
(44) Materials Data, Inc., 1224 Concannon Blvd., Livermore, CA 94550, U.S.A.

Table 2. Parameters for Rietveld Refinement[45] [a]

modeling parameter	NiO (bunsenite) 44-1159	nickel aluminate 10-339	γ-alumina 10-0425	δ*-alumina 46-1215	θ-alumina 23-1009
system	cubic	cubic	cubic	orthorhombic	monoclinic
space group	$Fm\bar{3}m$ (225)	$Fd\bar{3}m$ (227)	$Fd\bar{3}m$ (227)	$P222$ (16)	$C2/m$ (12)
a, Å	4.177	8.048	7.90	7.934	11.813
b, Å	4.177	8.048	7.90	7.956	2.906
c, Å	4.177	8.048	7.90	11.711	5.625

[a] ICDD files shown below phase.

were added and ground again. The ground samples were packed firmly in the sample holder, leveled off at the upper edge to provide a smooth surface. The sample chamber was flushed continuously with N_2 to remove atmospheric CO_2. Each spectrum is continuous in the range 4000−400 cm^{-1} with a scan resolution of ±4 cm^{-1} with an average of 130 scans. A new reference sample (400 mg of ground KBr) was made every five samples.

Results and Discussion

The objective of the work reported here is to demonstrate that LF-FSP processing can provide high surface area (>40 m^2/g), mixed-metal oxide nanopowders without microporosity, along the NiO−Al_2O_3 tie line with the goal of generating materials with compositions known to offer good catalytic properties with atomic mixing of the precursor ions.[1−5] The absence of microporosity is important given that many high surface area catalysts (>50 m^2/g) made using sol−gel techniques and/or by impregnation of microporous supports suffer from aging processes wherein the micropores are removed during aging by sintering processes, which in turn remove active metal initially deposited within the micropores. Furthermore, because the high surface area is achieved by making catalyst particles with very small diameters, much of the catalyst material is at the particle surface, in principle, ensuring that the major portion of the metal species that could be active can in fact contribute to catalyst activity.

The downside to this approach is that in some instances, catalyst recycling may be difficult because of the difficulty in recovering the catalyst particles. However, where high activity is obtained, it may not be necessary to recover the catalyst if it is used in small amounts. Alternately, many applications involve gas- or liquid-phase reactions where the gaseous reactants and/or products may be separated even from fine particulates. One potential solution to this problem is to very lightly sinter (promote limited necking between particles) these active species to retain the high surface area of the primary particles while limiting their mobility. However, such issues are not an immediate concern of the work reported here.

Spinels are a common structural arrangement shared by many transition metals oxides of the general formula AB_2O_4. These structures can be further divided into three types: normal, inverse and intermediate spinels.[30,31] They all consist of a cubic close-packed (face-centered) sublattice of oxygen atoms with 1/8 of the tetrahedral sites and 1/2 of the octahedral sites occupied by the cations. The distinction between normal and inverse lies in which atoms occupy which positions.

In normal spinels, the tetrahedral (A sites) are occupied exclusively by divalent cations and octahedral (B sites) are occupied by trivalent cations. In an inverse spinel, half of the trivalent cations replace the divalent cations so that divalent cations now occupy octahedral sites giving rise to the formula $B^{3+}(A^{2+}B^{3+})O_4$. The intermediate spinels have partial normal and partial inverse character and are normally labeled in terms of the percent inverse character they exhibit.[32,33]

The ability to predict formation of normal or inverse spinels has been of considerable interest since the 1930s when both structures were first observed. O'Neil and Navrotsky[34,35] have published a set of studies that examine factors such as electrostatic interactions, ligand field effects, and atomic radii on spinel cation distribution patterns. Cormack et al.[36] found through simulations based on electrostatic and short-range contributions, ion size, site preference energies, and coordination number that Ni^{2+} strongly prefers to occupy octahedral positions.

These findings are supported by studies on $NiCr_2O_4$[37] and $NiFe_2O_4$[38] that show that Ni^{2+} tends to force formation of inverse spinel phases.[39−41] In the current studies we find that the inverse spinel phase can "saturate" at high Ni contents, with the divalent cation driving formation of intermediate spinels. Furthermore, at very low Ni^{2+} contents (LF-FSP produced samples with 22 and 43 mol % NiO) a single-phase intermediate spinel forms where some Al^{3+} ions must occupy octahedral sites normally occupied by Ni^{2+} (all the Ni is still occupying some of the octahedral sites), especially in the former case where the phase diagram suggests that a single phase should not form. Hence, the 22% NiO material represents a new phase composition along the NiO−Al_2O_3 tie line. We begin by discussing the basic formulation of the catalyst precursor solutions, then move on to production of nanopowders from these precursors, and follow with characterization of the LF-FSP products.

Precursor and Precursor Formulations. We have previously reported the detailed characterization of alumatrane, $Al(OCH_2CH_2)_3N$, and its utility in generating high surface area, unagglomerated nano-δ-Al_2O_3.[24] Thus, we report only on the nickel propionate, which has a thermal decomposition pattern similar to those of other metal carboxylate precursors we have examined.[21b] Figure 1 is a TGA trace which shows an initial mass loss (≈14%) event commensurate with the loss of ≈0.5 equiv of propionic acid of recrystallization.

The second mass loss at 250−300 °C is attributed to decomposition of the propionate ligands. This mass loss is 37.2% of the total mass at this point and within experimental error of the calculated value (36.5%) for decomposition of $Ni(O_2CCH_2CH_3)_2$ to NiO and is expected on the basis of previous studies on the thermal decomposition of metal carboxylates.[21b]

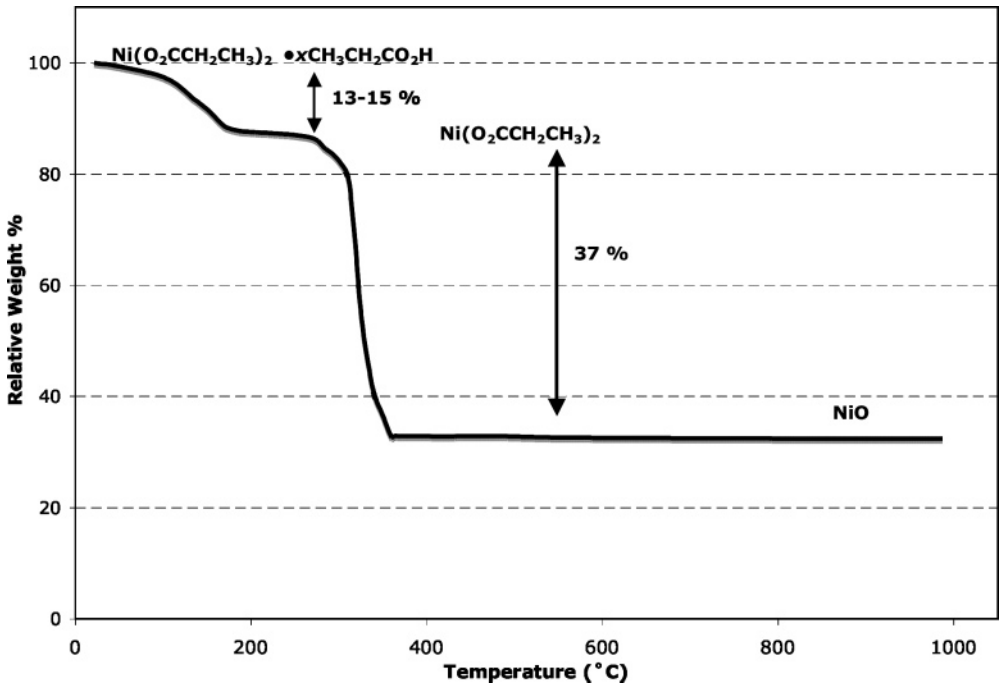

Figure 1. TGA of $Ni(O_2CH_2CH_3)_2$ ramped at 10 °C/min in synthetic air.

Table 3. Energy Values of Solvent Vehicles Used[46]

	methanol	ethanol	butanol
energy value (kJ/L)	−17 930	−23 600	−29 260
50:50 vol with EtOH (kJ/L)	−20 760	−23 600	−26 430
energy value (kJ/mol)	−730	−1370	−2670
50:50 mol with EtOH (kJ/mol)	−1050	−1370	−2020

The final TGA product was verified by XRD (not shown) to be NiO, confirming the suggested thermally promoted fragmentation of the two propionate ligands. The initial loss, attributed to propionic acid, indicates that the precursor prepared as described in Experimental Section is $Ni(O_2CCH_2CH_3)_2 \cdot xCH_3CH_2CO_2H$ where $x = 0.4-0.5$.

Eight different precursor compositions were prepared to study the $NiO-Al_2O_3$ system; Table 1 lists the various compositions studied. Measured amounts of precursor/EtOH solutions were prepared such that the total ceramic loading (as precursor) in solution was 2.0−4.0 wt %, typically 3 wt %. All precursor systems thus formulated exhibited viscosities close to those of EtOH, thereby minimizing potential problems with aerosolization. The compositions of all eight LF-FSP samples were corroborated by Galbraith Laboratories (Knoxville, TN) using ICP and at Ford Motor Co. SciLab (Dearborn, MI) using XRF.

Solvents/Fuels. Three different batches of sample 2 (3 mol % NiO in Al_2O_3) were produced using different solvent/fuel combinations. The first used pure EtOH, the second a 50:50 mol % MeOH/EtOH, and the last 50:50 mol % ^{n}BuOH/EtOH. The object was to control the flame temperature by changing the fuel heats of combustion (Table 3) in an effort to affect APSs and morphologies.

We consistently find[24] that different solvent/fuel combinations produce nearly identical powders as determined by XRD powder patterns and particle morphologies (SEM, TEM). Likewise, TGA and DTA data show no significant difference between the samples. The SSAs are, within error limits, all the same. Hence, efforts to change particle morphology via variations in flame temperatures appear not to make a difference. This suggests that it is the rapid quenching process in LF-FSP that defines particle morphologies.

In general, the temperatures at the exit to the 1.25 m (0.20 m diameter) quartz combustion chamber are 400−500 °C, corresponding to a drop of 1000−1500 °C in a 1 m length depending on the processing conditions. At these quenching rates, the gas-phase ions produced during combustion have, as we have discussed elsewhere,[20−25] microseconds to cool and condense. Thus, the time for these species to form nuclei is very limited. Indeed, the time is sufficiently limited that uniform stoichiometries reflecting the original solution stoichiometries are almost always observed. Furthermore, the time for collisions between growing nuclei at temperatures that produce particle necking that in turn would lead to hard agglomerates is also limited. Thus, the product powders are typically single particles with very few necks. Surprisingly, this quenching rate rarely leads to glassy products.

Powder Characterization. All LF-FSP powders were characterized by BET, SEM, TEM, XRD, TGA-DTA, and DRIFTS as discussed in the following sections. These characterization tools allow us to better understand particle morphologies, sizes and distributions, phase composition, surface areas, and chemistries.

Surface area analyses. SSAs of the as-produced powders were obtained by the BET method (see Experimental Section) and used along with XRD peak broadening to estimate particle sizes; see Table 4. No microporosity was expected nor detected by the *t*-plot method. With the exception of the pure NiO powders, the SSAs at all compositions exceed 45 m^2/g. At some compositions along the $NiO \cdot Al_2O_3$ tie line, the observed SSAs are up to 30% greater than pure δ-Al_2O_3 (80 vs 60 m^2/g). Consequently, the APSs decrease with the addition of NiO as compared to pure alumina, because particle nucleation and growth must be influenced by the materials composition such that growth is inhibited.

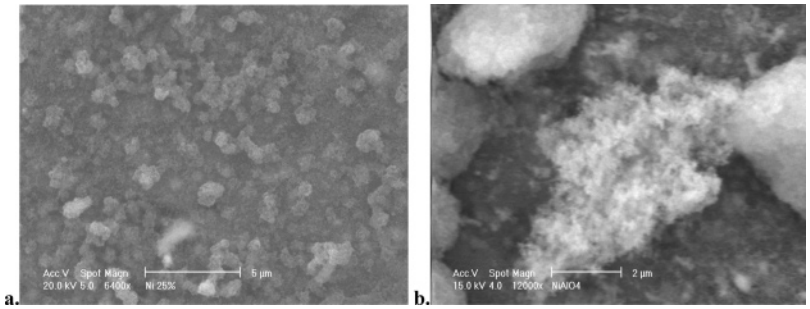

Figure 2. SEM micographs for (a) sample 4, 22 mol % NiO, and (b) sample 5, 43 mol % NiO.

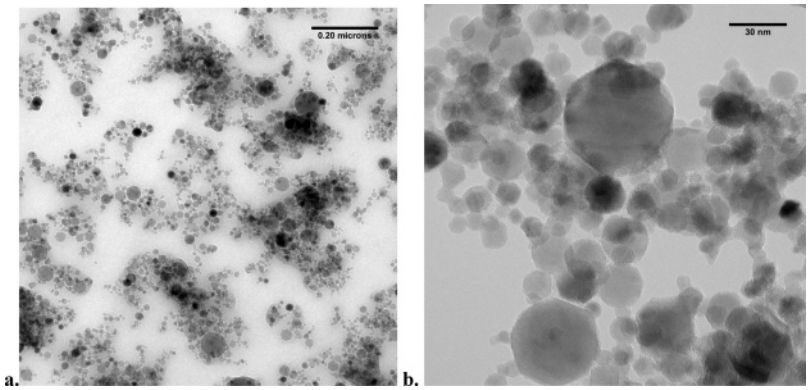

Figure 3. HRTEM micrographs showing the sample 4, 22 mol % NiO, (a) distribution of particles throughout the sample and (b) specific weak agglomerate demonstrating APS < 30 nm.

Table 4. Surface Areas and APSs of Powders

	sample	SSA (m^2/g)	theor density (g/cm^3)[a]	APS (nm) BET[b]	APS (nm) XRD
1	Al_2O_3	57	3.65	29	29
2	3 mol % NiO	60	3.74	27	23
3	5 mol % NiO	77	3.77	21	19
4	22 mol % NiO	60	4.16	24	18
5	43 mol % NiO	69	4.76	18	20
6	63 mol % NiO	58	5.33	19	22
7	78 mol % NiO	45	5.86	23	20
8	NiO	7	6.72	134	62

[a] Calculated by percent of species (NiO, $NiAl_2O_4$, Al_2O_3) present, error ± 0.02. [b] Using formula 1, error ± 0.5.

The melting temperature (T_m) for $NiO{\cdot}Al_2O_3$ is ≥2100 °C, whereas T_m for Al_2O_3 is <2000 °C. If the boiling points and/or sublimation or condensation temperatures for these materials follow suit, one might argue that under identical LF-FSP conditions, $NiO{\cdot}xAl_2O_3$ nuclei will form from the gas phase and/or cease growing, nucleating, or coalescing at higher temperatures than pure Al_2O_3. This is one possible explanation for the higher average surface areas/smaller particle sizes.

SEM. SEM micrographs of as-prepared nanopowders (Figure 2) were used to assess the overall particle distribution and morphology of each sample. All the powders exhibit similar spherical and homogeneous morphologies. The APSs are all <80 nm, with a significant population of particles < 60 nm. Figure 2a provides an overview of the general particle population that allows one to conclude that no micron size particles are produced during LF-FSP of these materials. However, Figure 2b indicates the presence of electrostatically agglomerated particles, as seen with pure δ-Al_2O_3, which disperses fully[47] despite the presence of these same types of agglomerates.

TEM. HRTEM images of sample 4, 22 mol % NiO, Figure 3, are representative of all other powder samples. Figure 3a captures the appearance of the general particle population at a length scale different from that seen by SEM. As stated above all of the particles are spherical, ≤80 nm in diameter with the majority <30 nm. Moreover, most particles are multi-faceted (Figure 3b), suggesting a high degree of crystallinity. Particle necking while evident is not a major morphological feature for the reasons discussed above. Figure 3b does not reveal any obvious microporosity, as expected from the *t*-plot results.

X-ray Powder Diffraction. X-ray powder diffraction patterns for the as-processed samples are given in Figure 4. Figure 5 shows the relevant ICDD powder patterns for NiO, $NiO{\cdot}Al_2O_3$, δ-Al_2O_3, and δ*-Al_2O_3 (44-1159, 10-0339, 46-1215, and 46-1131 respectively). Debye−Scherrer XRD line-broadening analyses give APSs consistent with the BET analyses (see Table 4). Samples with up to 5 mol % NiO show at most traces of crystalline $NiAl_2O_4$. These powders exhibit a blue cast that increases in intensity with increasing Ni^{2+} content associated with the formation of inverse nickel spinel.

As more NiO is added, the three main peaks at 37, 45, and 66° 2θ for cubic spinel phase $NiO{\cdot}Al_2O_3$ (ICDD 10-0339) gradually increase in intensity as $NiO{\cdot}Al_2O_3$ spinel becomes the sole phase near the correct stoichiometry. At very high nickel contents of 63 and 78 mol % NiO, LF-FSP finally generates powders with mixed phases of $NiO{\cdot}Al_2O_3$ and NiO.

(45) *The Rietveld Method*; Young, R. A., Ed.; Oxford University Press: New York, 1997.
(46) Rossini, F. D. *J. Res. Natl. Bur. Stand. (U.S.)* **1934**, *13*, 189−197.
(47) Bell, N. S.; Rodriguez, M. A. *J. Nanosci. Nanotech.* **2004**, *4*, 283.

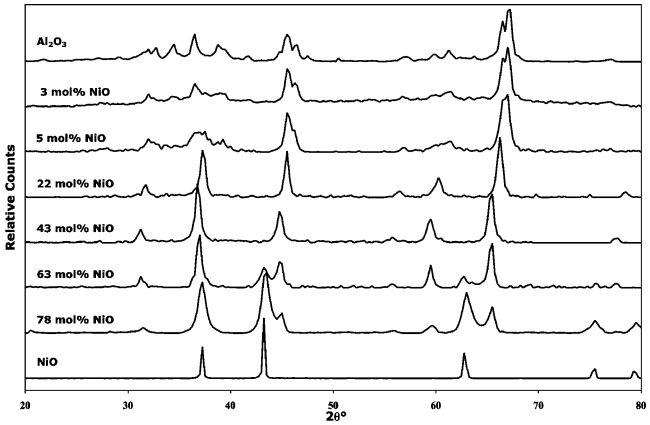

Figure 4. XRD patterns of all samples, showing the appearance of NiO·Al_2O_3 (ICDD 10-0339). The XRD peak shifts result from formation of inverse and intermediate spinels.

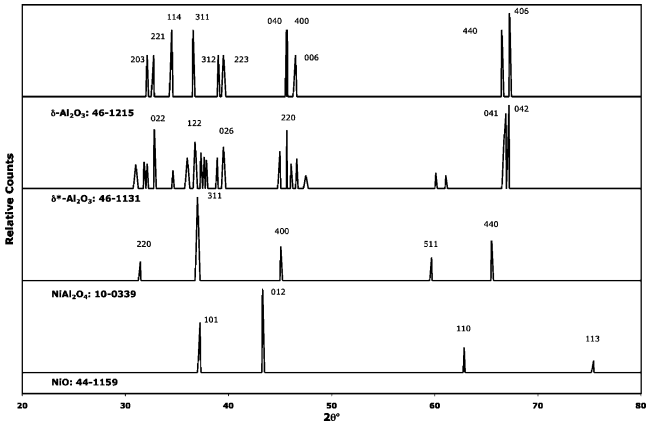

Figure 5. ICDD powder diffraction patterns for NiO, $NiAl_2O_4$, and Al_2O_3 for comparison with the Figure 4 data.

Sample 4, with 22 mol % NiO, does not exhibit the XRD powder pattern expected based on the phase diagram which is a mixture of corundum (α-alumina) and phase pure NiO·Al_2O_3, nickel spinel.[48] Initially, we thought that there was a compositional mistake in formulating the precursor, making it closer to phase pure nickel spinel; however, chemical analyses by ICP and XRF were reproducible. During the period when the chemical analyses were being done, we also thought that the powder pattern was misaligned in the stack shown in Figure 4. However, the use of a Si standard confirmed the unusual 4° 2θ shifts. Five separate samples were made at this composition to ensure reproducibly.

Vegard's law was used to calculate unit cell parameters for the sample 4 materials (see Experimental Section). By taking the pure species as the end compounds, sample 4 (22 mol % NiO), with 37 mol % excess Al_2O_3, should have a cubic cell parameter of 0.7996 nm versus 0.8011 nm found here. Thus this material exhibits a positive deviation from Vegard's law.

Vegard's law is an empirical method of assessing the changes in unit cell parameters associated with vacancies in mixed-metal, metal-oxide, and, recently, semiconductor materials. There are numerous ways to interpret these data, none of which appear to be completely satisfactory.[49−51] We believe that the simplest explanation is that the presence of Al^{3+} ions in positions normally filled by Ni^{2+} ions implies that there are vacancy sites where only oxygen anions are present and it is the resulting electrostatic repulsion that leads to the somewhat larger unit cell parameters. However, this will require more work to confirm.

More interesting is the single phase present. According to Phillips et al.,[48] sample 4, with 22 mol % NiO, should exhibit two phases, the spinel structure and α-Al_2O_3. Rietveld refinement (see Figure 6) of sample 4 shows that indeed it is a single phase inverse spinel, with Al occupying all A sites and the B site having a 13% Ni and 87% Al occupancy. The formula for this material from crystallographic information gives rise to the formula $Al_{1.0}(Al_{1.74}Ni_{0.26})O_4$. Silicon (20 wt %) was added as the internal standard accounting for a 103% recovery in the refinement. This is used to verify the position of the background trace to screen for phases that lack long-range order. Alumina and γ-Ni accounted for 87 wt % (novel spinel phase) with an average crystallite size of 170 Å, and an amorphous phase was detected and accounted for 13 wt % of the sample. Furthermore, TGA-DTA studies designed to observe the expected phase segregation process did not lead to any observed changes in the XRD pattern after heating to 1400 °C; see below.

Thus, LF-FSP processing appears to offer access to a new stable inverse spinel along the NiO−Al_2O_3 tie line. These results coupled with our recent discovery of a new phase of $Y_3Al_5O_{12}$ composition[25] suggest that LF-FSP not only offers an excellent method of making high quality mixed-metal oxide nanopowders but also offers the opportunity to create new phases (materials) or novel extensions of known phases.

The most likely explanation is that the high homogeneity of atomic mixing in the flame coupled with extremely fast formation and quenching of particles leads to unusual kinetic phases. However, atomic mixing in the flame is insufficient to produce high quality powders, and the chemistry of the precursor is very important in determining the quality and type of nanopowder produced.[24]

TGAs. TGAs of the eight as-prepared powders were run to determine the relative quantities of various surface species including physisorbed and chemisorbed water, carbonate species, and possibly hydrocarbons synthesized perhaps by steam reforming during LF-FSP (see FTIR data). All powders exhibit typical[24] 1−4 wt % mass losses over the 1200 °C ramp range (Figure 1, Supporting Information).

As noted above, nitrogen adsorption analyses do not indicate the presence of microporosity for any of the powders produced. One consequence of this is that they exhibit far less hydration than microporous powders.[24,52] The majority of this mass loss is due to thermal elimination of both physi- and chemisorbed water on the particle surfaces, which arises from the combustion process. Likewise, smaller mass losses are in general attributed to loss of CO_2 from the surfaces of the powders entrained during combustion.

(48) Phillips, B.; Hutta, J. J.; Warchaw, A. *J. Am. Ceram. Soc.* **1963**, *46*, 581.
(49) Lubarda, V. A. *Mech. Mater.* **2003**, *35*, 53.
(50) Chhaya, U. V.; Kulkarni, R. G. *Mater. Lett.* **1999**, *39*, 91.
(51) Sano, T.; Tamaura, Y. *Mater. Res. Bulletin* **1999**, *34*, 389.
(52) McHale, J. M.; Navrotsky, A.; Perrotta, A. J. *J. Phys. Chem. B* **1997**, *101*, 603.

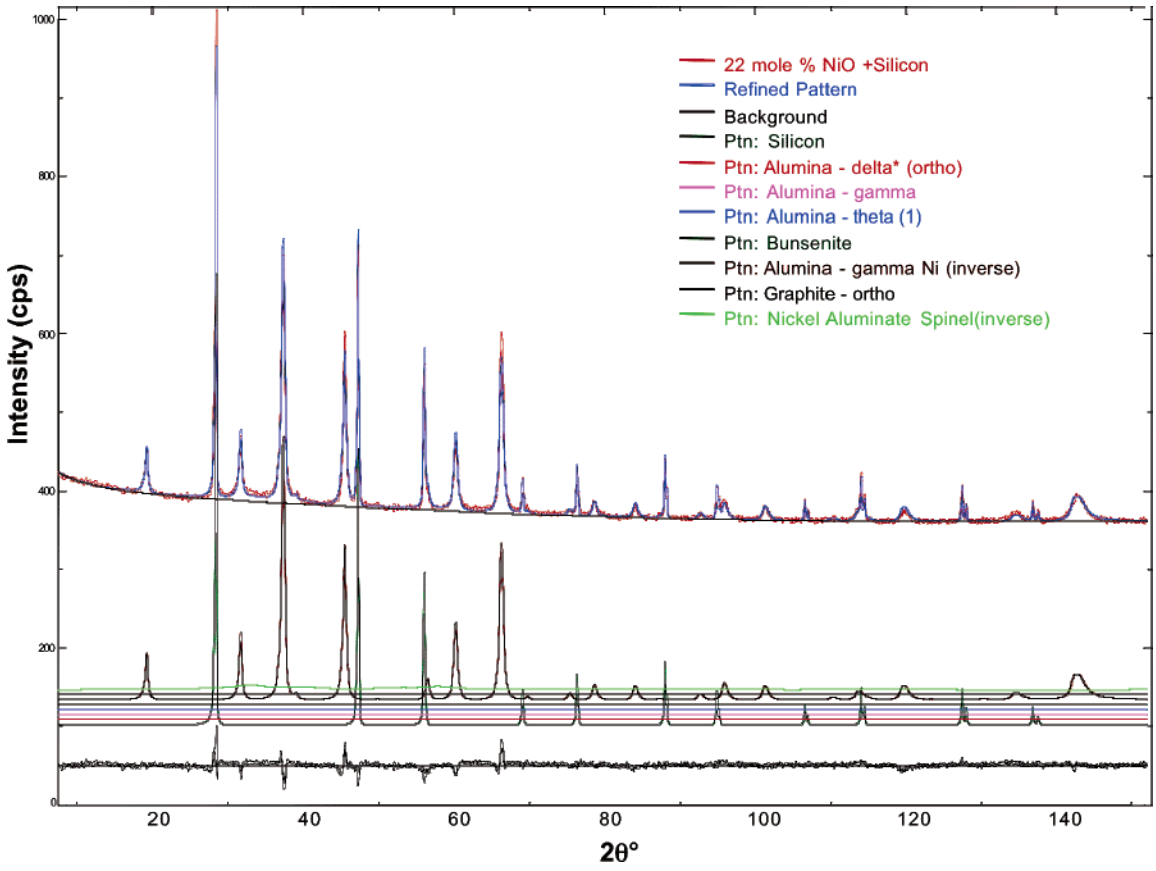

Figure 6. Rietveld refinement plot for sample 4.

All samples behave very similarly with gradual mass losses over the 100 to 500 °C range that, within the error limits of the analysis of these high SSA powders, are all similar to pure δ-Al_2O_3. The two exceptions are sample 8, pure NiO, which has a relatively low SSA of 7 m^2/g and an associated mass loss of $\leq$1 wt %, and sample 6. At 63 mol % NiO, sample 6 has the highest surface area per metal content and exhibits a distinct 3 wt % mass loss at $\approx$300 °C. This may simply be a consequence of sample handling. However, there appear to be residual organic species (see FTIR below) for some of the higher NiO content samples that may result from steam reforming leading to hydrocarbon formation during LF-FSP. In pure δ-Al_2O_3 samples of the same SSA, no such peaks are observed for samples produced over a 5-year period.

DTA (Not Shown). DTA shows no major phase transformations up to 1300 °C. The sample traces show little variance, indicating the excellent thermal stability of considerable value for electrode and catalytic applications. Added NiO delays phase transformation to α-Al_2O_3 usually seen at $\sim$1200 C. Samples 4−6 (22, 43, and 63 mol % NiO, respectively) do not transform to α-Al_2O_3 (per XRD) even on heating to 1400 °C.

DRIFTS. DRIFTS spectra of as-prepared powders were run (Figures 2 and 3, Supporting Information). The spectra are not particularly revealing and generally follow those observed for pure δ-Al_2O_3. In the 3700−2500 cm^{-1} region, weak νOH bands are observed attributable to surface hydroxyls on alumina[53,54] arising from both physi- and chemisorbed water. In the 2900−2700 cm^{-1} region small νCH bands are observed primarily for the 43 and 63 wt % materials indicating some surface organic species. These bands are associated with a 2% mass loss seen at >300 °C for sample 6 (Figure 1, Supporting Information). In the 1800−1200 cm^{-1} region, we observe weak bands due to carbonate species[55] again in accord with those seen for pure δ-Al_2O_3.[24a]

The 1000−400 bands are typical for νM−O band. δ-Al_2O_3 has two νAl−O bands at 810 and 610 cm^{-1}.[56] Nickel oxide has a well-defined νNi−O centered around 500 cm^{-1}.[57] Figure 3 (Supporting Information) shows a steady decline in the νAl−O band intensities, broadening and an increase of the band attributed to νNi−O.

Conclusions

LF-FSP offers the opportunity to produce mixed-metal oxide nanopowders with exceptional control of stoichiometry, phase, and phase purity. LF-FSP also provides the potential to access entirely new phases heretofore not observed by standard catalyst and nanopowder synthesis techniques. In this paper we used LF-FSP to produce a series of powders along the NiO−Al_2O_3 tie line. LF-FSP provides access to materials with what appears to be atomic mixing within nanometer length scales. Prior to the work reported here,

(53) Lee, D. H.; Condrate, R. A. *Mater. Lett.* **1995**, *23*, 241.
(54) Saniger, J. M. *Mater. Lett.* **1995**, *22*, 109.
(55) Surca, A.; Orel, B.; Pihlar, B.; Bukovec, P. *J. Electroanal. Chem.* **1995**, *83*, 408.
(56) Tarte, P. *Spectrochim. Acta, Part A* **1967**, *23*, 2127.
(57) Biju, V.; Khadar M. A. *Spectrochim. Acta, Part A* **2003**, *59*, 121.

this has proven to be very difficult to do for materials along the $NiO-Al_2O_3$ tie line.[17−19] The probable explanation is that the thermal stability of the materials produced is so high (no phase transformations seen at 1400 °C) that, once partially formed, further diffusion of atomic species is so slow that equilibration of thermodynamically favored phases is very slow or essentially impossible without special heat treatments to very high temperatures. This then greatly reduces surface areas, making the resulting materials useless for catalyst applications. We find that the addition of NiO reduces the final particle sizes considerably as evidenced by increases in SSAs by as much as 30% (from 60 to 80 m^2/g). The increase in SSA is likely a consequence of the higher thermal stability of the solid that nucleates out of the gas phase during the FSP process.

Because LF-FSP involves rapid quenching of the combustion species, it appears to offer access to new, kinetic phases not accessible by standard processing techniques. Our observation of a new composition for an inverse spinel at $(NiO)_{0.22}(Al_2O_3)_{0.78}$ far outside the currently accepted stable spinel compositions for this system supports this idea. However, $(NiO)_{0.22}(Al_2O_3)_{0.78}$ nanopowders are surprisingly robust and survive heating in air to 1400 °C where, based on the phase diagram,[54] this material might be expected to be metastable. As stated above, one might argue that the very high T_m's for these systems make it difficult if not impossible to actually reach thermodynamic equilibrium for these materials.

In future papers we will demonstrate the utility of LF-FSP for producing materials along the $CeO_2-Al_2O_3$ and $ZrO_2-Al_2O_3$ tie lines and mixed-phase materials in the $CeO_2/ZrO_2/Al_2O_3$ ternary and $CeO_2/ZrO_2/NiO/Al_2O_3$ quaternary systems where it is possible to generate three-way auto-exhaust washcoat materials and steam reforming catalysts in one step using LF-FSP.

Acknowledgment. We thank AFOSR for support of this work through Contract No. F49620-03-1-0389. P.S. thanks NSF for an IGERT Fellowship (DGE-9972776) for support for this work. We would also like to thank Maxit Corporation for partial support of this work. J.A.A. would like to thank Ford Motor Company and Dr. Christopher Goralski Jr. for summer fellowships supporting this work and useful discussions. We would especially like to thank Mark J. Jagner at Ford Motor Company for all the help in XRF analysis.

Supporting Information Available: TGA of samples heated at 10 °C/air to 1200 °C and DRIFTS spectra of all samples (PDF). This material is available free of charge via the Internet at http://pubs.acs.org.

CM0503026